doi:10.1246/cl.2012.708
Published on the web June 23, 2012

Improvement of Thermal Stability of Gold Nanoparticles by Synergistic Interligand Interactions

Atsushi Okumura,[1] Yoshitaka Tsuchido,[1] Kou Yamada,[2] Kenji Todori,[2] and Shigeru Machida*[1]
[1]*Tokyo National College of Technology, 1220-2 Kunugida-machi, Hachioji, Tokyo 193-0997*
[2]*Corporate Research and Development Center, Toshiba Corporation, 1 Komukai-Toshiba-cho, Saiwai-ku, Kawasaki, Kanagawa 212-8582*

(Received March 21, 2012; CL-120242; E-mail: smachida@tokyo-ct.ac.jp)

Three types of novel gold nanoparticles containing a different condensed ring in their ligands were prepared. Their thermal stability was found to be much higher than that of typical gold nanoparticles surrounded by long-chain alkanethiols because of strong interligand interaction formed by the condensed rings (π–π stacking). A clear correlation was found between the thermal stability and the strength of π–π stacking.

Recently, gold nanoparticles have been extensively investigated owing to their characteristic behavior compared to bulk gold.[1–4] Since gold nanoparticles have a strong affinity, they are generally surrounded by organic molecules called ligands that prevent the nanoparticles from aggregating. Brust et al. reported that gold nanoparticles surrounded by long-chain alkanethiols **1** show high dispersibility in nonpolar organic solvents and do not aggregate even in the solid condition.[5] The thiol group anchors the ligand molecule to the surface of the gold core, while the long-chain alkyl groups interact intermolecularly with each other by van der Waals forces and stabilize the gold core. However, since the van der Waals interaction is weak, the gold nanoparticles surrounded by the typical long-chain alkanethiols need to be improved in terms of their thermal resistance.

Therefore, with the aim of developing thermally resistant gold nanoparticles, we focused on functional groups such as the amide group and aromatic rings. In our previous study,[6] ligands containing an amide group and/or a tolyl group (Figure 1) were synthesized, and the thermal stability of the corresponding gold nanoparticles was evaluated by thermogravimetry (TG). It was found that the gold nanoparticles with a tolyl group in their ligands **3** and **4** did not aggregate up to about 300 °C. This result suggests that introducing aromatic rings into ligands is effective for enhancing the thermal stability.

Therefore, in this study, we synthesized three novel ligands containing condensed rings (Figure 2), with the aim of further improving the thermal stability. Gold nanoparticles were then prepared with these ligands, and their thermal stability was evaluated based on TG analysis.

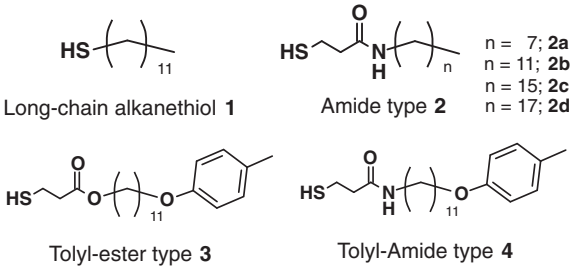

Figure 1. Chemical structures of long-chain alkanethiol **1** and synthesized ligands **2**, **3**, and **4**.

The synthetic routes for ligands **5**, **6**, and **7** are shown in Schemes 1, 2, and 3, respectively. 3-(Tritylthio)propanoic acid was synthesized according to Polidori et al.'s method.[7] Tetrahydrofuran (THF) was purified by distillation and stocked under a nitrogen atmosphere. Other chemicals were used without further purification.

^{1}H NMR spectra were measured using a JEOL AL-400, and infrared absorption was measured with a JASCO FT/IR-620.[8]

All of the gold nanoparticles **Au-5**, **Au-6**, and **Au-7** were prepared in accordance with the Brust et al. method.[5] Perylene-type (**Au-6**) and coronene-type (**Au-7**) gold nanoparticles were found to disperse in chloroform, while pyrene-type (**Au-5**) gold nanoparticles readily dispersed in chloroform as well as toluene.

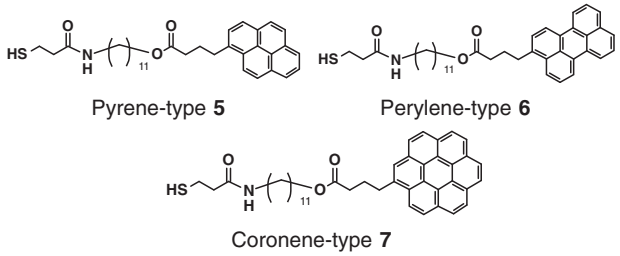

Figure 2. Chemical structures of novel ligands **5**, **6**, and **7**.

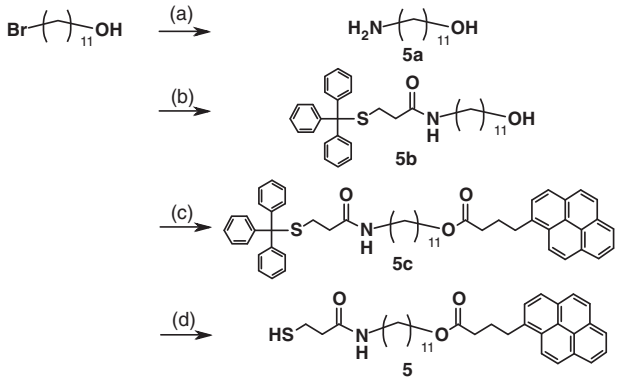

Scheme 1. Synthetic route for pyrene-type ligand **5**: (a) NaN_3, CH_3CN, reflux, overnight, then $LiAlH_4$, THF, 0 °C, 1 h; (b) 3-(tritylthio)propanoic acid, 1-ethyl-3-(3-dimethylaminopropyl)-carbodiimide hydrochloride (EDC), 4-dimethylaminopyridine (DMAP), CH_2Cl_2, rt, overnight; (c) 1-pyrenebutanoic acid, EDC, DMAP, CH_2Cl_2, rt, overnight; (d) trifluoroacetic acid, triethylsilane, rt. Total yield of the four steps: 20%.

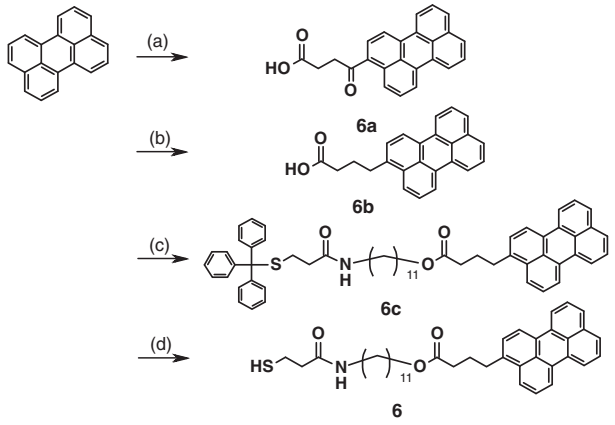

Scheme 2. Synthetic route for perylene-type ligand **6**: (a) succinic anhydride, $AlCl_3$, CH_2Cl_2, rt, 13 h; (b) N_2H_4 (79% hydrate), NaOH, diethylene glycol, reflux, 4 h; (c) compound **5b**, EDC, DMAP, CH_2Cl_2, rt, overnight; (d) trifluoroacetic acid, triethylsilane, rt. Total yield of the four steps: 17%.

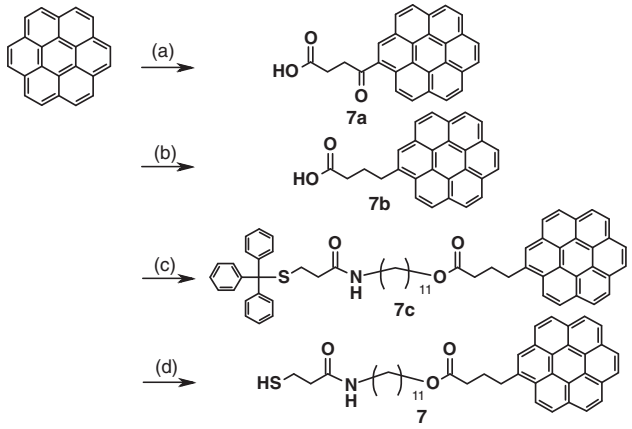

Scheme 3. Synthetic route for coronene-type ligand **7**: (a) succinic anhydride, $AlCl_3$, nitrobenzene, rt, 5 h; (b) N_2H_4 (79% hydrate), NaOH, diethylene glycol, reflux, 4 h; (c) compound **5b**, EDC, DMAP, CH_2Cl_2, rt, overnight; (d) trifluoroacetic acid, triethylsilane, rt. Total yield of the four steps: 15%.

Gold nanoparticles are known to have a broad absorption range of 450–600 nm, which is attributed to the surface plasmon resonance of the Au cores. Therefore, UV–vis absorption spectra were measured using a SHIMADZU UV-3600 to confirm the generation of the gold nanoparticles. Figure 3 shows the absorption spectrum of the pyrene-type gold nanoparticles **Au-5**, where the broad absorption attributed to the surface plasmon resonance was observed in the 450–600 nm range. Similar absorption was also confirmed in the spectra of the other gold nanoparticles **Au-6** and **Au-7**.

Particle sizes of the gold nanoparticles were estimated on the basis of transmission electron microscopy (TEM) images taken with JEOL JEM-2000EX. Figure 4 shows the TEM image of **Au-5**; its average size was visually estimated to be ca. 2 nm. The other gold nanoparticles were found to be about the same size as **Au-5**. The calculated standard deviations of **Au-5**, **Au-6**, and **Au-7** were 0.3, 0.4, and 0.7 nm, respectively, and their size distributions were similar in shape.

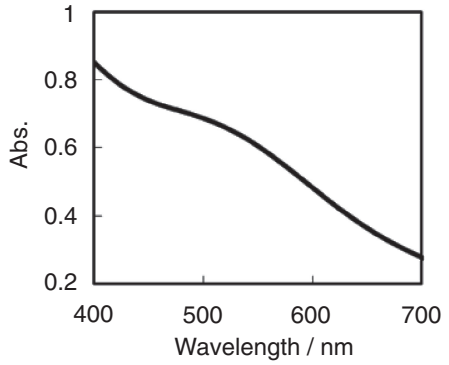

Figure 3. UV–vis absorption spectrum of gold nanoparticles **Au-5**.

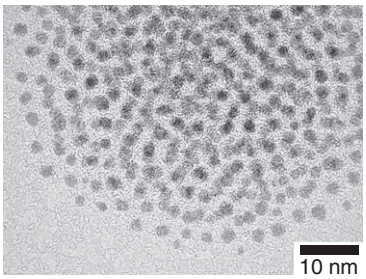

Figure 4. TEM image of gold nanoparticles **Au-5**.

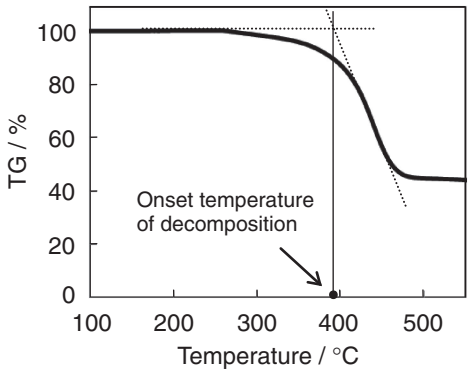

Figure 5. TG chart of gold nanoparticles **Au-5**.

In order to evaluate the thermal stability of the gold nanoparticles, TG measurements were carried out using SII TG/DTA 6300 at a heat rate of 20 °C min^{-1} under a nitrogen environment (150 mL min^{-1}).

Figure 5 shows the TG chart of **Au-5**, where the weight loss was observed in one step, owing to desorption of the ligand molecules from the gold surface. Since similar TG curves were obtained for the other gold nanoparticles, the onset temperature of decomposition was defined as shown in Figure 5. This temperature was then used as an indicator of the thermal stability of each gold nanoparticle (Figure 6).

The three novel gold nanoparticles **Au-5**, **Au-6**, and **Au-7** containing condensed rings showed a remarkably high onset temperature of decomposition in comparison with the others. Among the three, the pyrene-type gold nanoparticle **Au-5** had

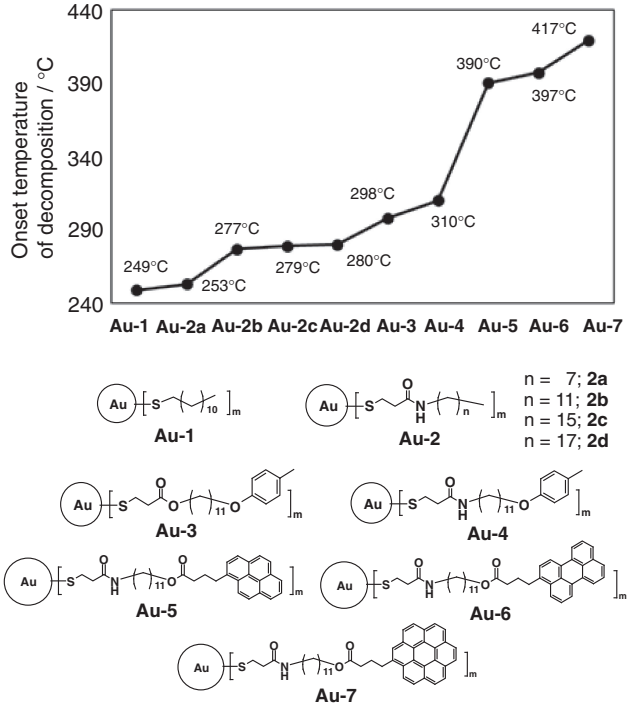

Figure 6. Onset temperature of decomposition of each gold nanoparticle.

Table 1. Correlation between the number of π electrons in each condensed ring and onset temperature of decomposition

Gold nanoparticle	Number of π electrons	Onset temperature of decomposition/°C	Weight loss/%
Au-5	16	390	59
Au-6	20	397	56
Au-7	24	417	57

the lowest thermal stability, followed by the perylene-type nanoparticle **Au-6**; the coronene-type nanoparticle **Au-7** had the highest stability. They were also found to have comparable amounts of ligands since their weight losses were of approximately the same value. Therefore, this result indicates that there is a clear correlation between the thermal stability and the number of π electrons (Table 1). Since the strength of the π–π stacking highly depends on the number of π electrons, there is a high degree of relativity between the π–π stacking strength and the thermal stability of the gold nanoparticles. Consequently, π–π stacking proved quite important for the development of thermally resistant gold nanoparticles.

In conclusion, three types of novel ligand molecules containing a different condensed ring were synthesized in order to evaluate the correlation between the strength of π–π stacking and the thermal stability of the corresponding gold nanoparticles. The onset temperature of decomposition was obtained based on TG analysis and used as an indicator of thermal stability. The temperature rose with an increase in π electrons. Therefore, π–π stacking was revealed to play an important role in the development of thermally resistant gold nanoparticles.

Figure 7 is a schematic illustration of the interligand interactions of the gold nanoparticles. The interligand hydrogen

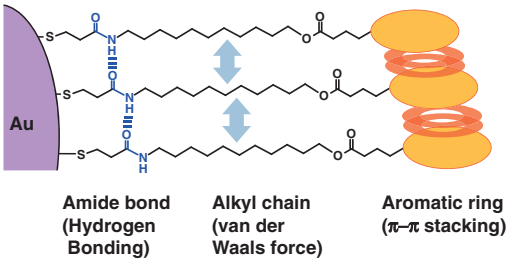

Figure 7. Schematic illustration of interligand interactions of novel gold nanoparticles **Au-5**, **Au-6**, and **Au-7**.

bonding is formed near the gold surface and stabilizes the orientation of the alkyl chain. This enables aromatic rings at the end of the ligand to readily form π–π stacking. This synergistic effect is considered to boost the contribution of π–π stacking to the enhancement of thermal stability.

This paper belongs to "Innovative Nanophotonics Components Development Project" which OITDA contracted with The New Energy and Industrial Technology Development Organization (NEDO) (2006–2010).

References and Notes

1 M.-C. Daniel, D. Astruc, *Chem. Rev.* **2004**, *104*, 293.
2 G. Schmid, B. Corain, *Eur. J. Inorg. Chem.* **2003**, 3081.
3 A. C. Templeton, D. E. Cliffel, R. W. Murray, *J. Am. Chem. Soc.* **1999**, *121*, 7081.
4 J. van Herrikhuyzen, R. A. J. Janssen, E. W. Meijer, S. C. J. Meskers, A. P. H. J. Schenning, *J. Am. Chem. Soc.* **2006**, *128*, 686.
5 M. Brust, M. Walker, D. Bethell, D. J. Schiffrin, R. Whyman, *J. Chem. Soc., Chem. Commun.* **1994**, 801.
6 Y. Tsuchido, K. Yamada, K. Todori, S. Machida, *Trans. Mater. Res. Soc. Jpn.* **2010**, *35*, 271.
7 A. Polidori, N. Michel, A. S. Fabiano, B. Pucci, *Chem. Phys. Lipids* **2005**, *136*, 23.
8 Spectroscopic data of **5**: ^{1}H NMR (400 MHz, $CDCl_3$): δ 8.31–7.84 (m, 9H, pyrene), 5.56 (br, 1H, NH), 4.08 (t, 2H, $J = 6.6$ Hz, CH_2OCO), 3.37 (t, 2H, $J = 7.8$ Hz, CH_2pyrene), 3.19 (q, 2H, $J = 6.7$ Hz, CH_2NH), 2.78 (q, 2H, $J = 7.3$ Hz, CH_2SH), 2.45 (m, 4H, CH_2CONH and CH_2COO), 2.18 (m, 2H, CH_2), 1.61 (m, 3H, SH and CH_2), 1.44–1.20 (br, 16H, CH_2); IR (KBr): 3304, 3038, 2920 (alkyl), 2850 (alkyl), 1726 (ester), 1638 (amide I), 1547 (amide II), 1467, 1263, 1177, 840, 720 cm^{-1}. Spectroscopic data of **6**: ^{1}H NMR (400 MHz, $CDCl_3$): δ 8.20–8.08 (m, 4H, perylene), 7.90 (d, 1H, $J = 8.3$ Hz, perylene), 7.67 (d, 1H, $J = 5.4$ Hz, perylene), 7.65 (d, 1H, $J = 5.1$ Hz, perylene), 7.52–7.43 (m, 3H, perylene), 7.32 (d, 1H, $J = 7.8$ Hz, perylene), 5.51 (br, 1H, NH), 4.08 (t, 2H, $J = 6.8$ Hz, CH_2OCO), 3.21 (q, 2H, $J = 6.7$ Hz, CH_2NH), 3.05 (t, 2H, $J = 7.8$ Hz, CH_2perylene), 2.79 (q, 2H, $J = 7.3$ Hz, CH_2SH), 2.43 (m, 4H, CH_2CONH and CH_2COO), 2.09 (m, 2H, CH_2), 1.61 (m, 3H, CH_2 and SH), 1.44–1.20 (br, 16H, CH_2); IR (KBr): 3301, 3053, 2920 (alkyl), 2853 (alkyl), 1726 (ester), 1635 (amide I), 1547 (amide II), 1465, 1188, 812, 768 cm^{-1}. Spectroscopic data of **7**: ^{1}H NMR (400 MHz, $CDCl_3$): δ 8.47–8.26 (m, 11H, coronene), 5.31 (br, 1H, NH), 4.09 (t, 2H, $J = 7.1$ Hz, CH_2OCO), 3.35 (t, 2H, $J = 7.8$ Hz, CH_2coronene), 2.98 (q, 2H, $J = 6.8$ Hz, CH_2NH), 2.67 (q, 2H, $J = 7.3$ Hz, CH_2SH), 2.51 (t, 2H, $J = 7.2$ Hz, CH_2CONH), 2.28 (m, 2H, CH_2), 2.20 (t, 2H, $J = 6.5$ Hz, CH_2COO), 1.59 (m, 2H, CH_2), 1.47 (t, 1H, $J = 8.3$ Hz, SH), 1.31–1.01 (br, 16H, CH_2); IR (KBr): 3287, 2919 (alkyl), 2849 (alkyl), 1728 (ester), 1633 (amide I), 1544 (amide II), 1465, 1176, 846, 544 cm^{-1}.

